J. Phys. Chem. A **1999,** *103,* 10764−10775

^{31}P and ^{23}Na Solid-State NMR Studies of Cation Dynamics in HT-Sodium Orthophosphate and the Solid Solutions $(Na_2SO_4)_x-(Na_3PO_4)_{1-x}$[†]

Michael Witschas and Hellmut Eckert*

Institut für Physikalische Chemie, Westfälische Wilhelms-Universität Münster,
Schlossplatz 7, D-48149 Münster, Germany

Received: August 4, 1999

The high-temperature phases of sodium orthophosphate, HT-Na_3PO_4, and of the solid solutions $(Na_2SO_4)_x-(Na_3PO_4)_{1-x}$ are characterized by their plastic crystalline state with dynamically disordered PO_4^{3-} and SO_4^{2-} anions and a remarkably high cation conductivity. Since HT-Na_3PO_4 possesses a fully occupied cation sublattice (no vacancies), it has been proposed that cation transport and anion reorientations are dynamically coupled ("paddle-wheel mechanism"). However, no direct evidence for this coupling has been reported. In the present study, the validity of this mechanism is investigated on the basis of ^{23}Na and ^{31}P nuclear magnetic resonance (NMR) experiments. Temperature-dependent measurements of the static ^{31}P linewidth indicate that in the solid solutions with $0.04 \leq x \leq 0.25$ the acceleration of sodium ionic mobility is closely correlated with the acceleration of phosphate rotational motion, associated with a second-order phase transition near 400 K. Temperature-dependent measurements of the ^{23}Na longitudinal and transverse relaxation times have been analyzed using the theory of quadrupolar relaxation under nonextreme narrowing conditions. Consistent with theoretical predictions sizeable dynamic frequency shifts are detected. All of the data are consistently analyzed quantitatively in terms of two distinct motional processes. A low-temperature process, whose relaxation strength is independent of sample composition, is clearly accelerated by the onset of fast anion rotation occurring at the second-order phase transition temperature. In addition, a high-temperature process, which is almost absent in HT-Na_3PO_4 but whose importance increases with increasing sulfate content, signifies vacancy hopping. This dependence on composition is easily understood because the substitution of PO_4^{3-} by SO_4^{2-} generates cation vacancies. The activation energies of both processes are near 0.45 eV, and the corresponding timescales grow increasingly similar with increasing sodium sulfate content. Altogether, the results give strong evidence for a dynamic coupling between anionic reorientation and cation diffusion, supporting the concept of a paddle-wheel mechanism.

Introduction

Among the large group of crystalline solid electrolytes there are a number of excellent cation conductors in the plastic crystalline state. In general, these materials are high-temperature phases of simple compounds such as Li_2SO_4, $LiNaSO_4$, and Na_3PO_4, where the anions are rotationally disordered and perform some kind of rotational diffusion.[1] An unresolved issue concerns the possibility of some dynamic coupling between both motional processes, leading to the proposal of a "paddle-wheel mechanism" in which the cations tumble through "revolving doors" represented by the anions.[1−7] This mechanism has been disputed by other authors, who instead favor a percolation type mechanism, where the increase of "free volume" as a consequence of a lattice expansion caused by the phase transitions is the main reason for conductivity enhancement.[8−12]

To resolve this literature controversy, it is necessary to study the dynamical characteristics of both anions and cations separately from each other on an atomic/molecular level. Thus, in the plastic crystalline material HT-Na_3PO_4 (HT indicates the high-temperature phase) temperature- and frequency-dependent electrical conductivity measurements have served to characterize the diffusive motion of the sodium cations,[13] whereas the rotational motion of the PO_4^{3-} anions has been probed by inelastic neutron scattering experiments.[14,15] Alternatively, nuclear magnetic resonance (NMR) techniques offer element-selective approaches for characterizing anion and cation motional processes in a separate fashion over a wide range of time scales. In general, atomic and molecular mobility on the time scale of milliseconds leads to stochastic averaging of the anisotropic static interactions influencing NMR spectra in the solid state. Thus, information on cation motion on the kilohertz timescale is available from a temperature-dependent measurement of static solid-state NMR spectra. Furthermore, temperature- and frequency-dependent measurements of nulcear spin−lattice relaxation rates afford a comprehensive characterization of the dynamics occurring on the megahertz timescale. During the past two decades, such NMR techniques have been employed to study ionic mobility in a wide variety of crystalline and glassy solid electrolytes,[16−19] also including some plastic crystalline conductors.[20,21] In the present study, we have used such techniques to characterize the cation dynamics in HT-Na_3PO_4 and its solid solutions with Na_2SO_4 in a quantitative, comprehensive manner. As will become evident, the effect of compositional variation on these lineshape and relaxation characteristics in the system $(Na_3PO_4)_{1-x}-(Na_2SO_4)_x$ provides important information regarding the identity and character of the motional processes studied.

Pure Na_3PO_4 undergoes a first-order solid−solid phase transition at 598 K from a low conducting tetragonal structure (LT (low-temperature) phase) to a highly conducting cubic modification (HT phase).[1] In this phase, which is stable up to the melting point, the rotationally disordered PO_4^{3-} anions form an fcc-lattice in which the sodium ions occupy all the tetrahedral and octahedral interstices.[22] The unit cell of the structure is shown in Figure 1. Because of the extremely high cation density, Na_3PO_4 easily forms solid solutions with structurally related compounds having lower cation densities. In particular, Na_2-

---

* To whom correspondence should be addressed.

[†] Dedicated to Professor Werner Müller-Warmuth on the occasion of his 70th birthday.

10.1021/jp992763i CCC: $18.00

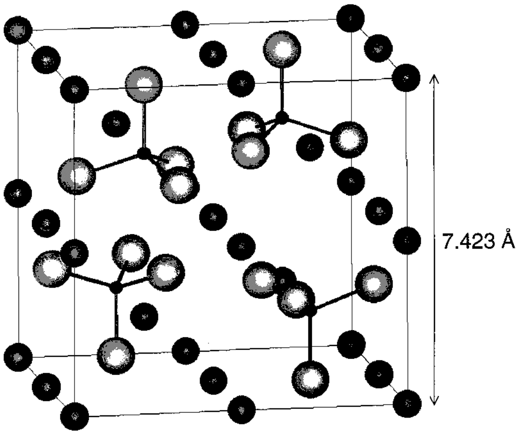

Figure 1. Representation of the unit cell of cubic HT-Na_3PO_4.

SO_4 is an ideal dopant material, because the sulfate and the phosphate ions are of comparable size, mass, and symmetry, and because the lattice constant does not change appreciably with dopant level.[23] Indeed, in $Na_3PO_4-Na_2SO_4$ solid solutions, the cubic phase can be stabilized down to room temperature.[23,24] Whether this phase is thermodynamically favored or merely metastable is uncertain at the present time, because no reliable phase diagram of this binary system exists.[25]

Concerning the issue of the paddle-wheel mechanism, the study of $Na_3PO_4-Na_2SO_4$ solid solutions offers important insights for two reasons. First of all, the extended region of stability offers a dynamical characterization of both anion and cation motion over a much wider range of timescales than possible in HT-Na_3PO_4. Second, significant changes in the transport mechanism may be expected in this system as the substitution level is changed. In pure HT-Na_3PO_4 all of the tetrahedral and octahedral sites are occupied with cations, making it hard to visualize percolation-type mechanisms. In the solid solutions, however, replacement of PO_4^{3-} by SO_4^{2-} anions creates Na^+ vacancies, the concentrations of which can be controlled by the substitution level. Therefore, in such solid solutions, defect- and percolation-type mechanisms of cation transport should become increasingly important as the sulfate concentration is increased. Thus, a systematic study of the dynamical ^{31}P and ^{23}Na NMR spectroscopic observables as a function of substitution level may offer important insights also into the ionic conduction mechanism in the Na_3PO_4 endmember.

Fundamental Concepts and Methodology

Influence of Sodium Motion on the ^{31}P Spin Hamiltonian. Useful information about the cation diffusion in Na_3PO_4 can be extracted by temperature-dependent monitoring of the ^{31}P NMR spectra. At low temperatures, where the cation diffusion is frozen out on the NMR time scale, the ^{31}P static lineshape is affected by both homonuclear $^{31}P-^{31}P$ and heteronuclear $^{31}P-^{23}Na$ dipole−dipole interactions. Using van Vleck theory,[26] the individual contributions of these interactions to the second moment can be computed on the basis of crystal structural data, using the internuclear $^{31}P-^{31}P$ and $^{31}P-^{23}Na$ distance distributions r_{ij} and r_{IS}, respectively.

$$M_{2d}(^{31}\mathrm{P}) = \underbrace{\frac{3}{5}\left(\frac{\mu_0}{4\pi}\right)^2 \gamma_{^{31}\mathrm{P}}^4 \hbar^2 I(I+1)\sum_{i>j} r_{ij}^{-6}}_{(a)} + \underbrace{\frac{4}{15}\left(\frac{\mu_0}{4\pi}\right)^2 \gamma_{^{31}\mathrm{P}}^2 \gamma_{^{23}\mathrm{Na}}^2 \hbar^2 S(S+1)\sum_{s} r_{IS}^{-6}}_{(b)} \qquad (1)$$

Here the γ_i are the gyromagnetic ratios, and I and S are the nuclear spin quantum numbers of ^{31}P and ^{23}Na, respectively. All the other symbols have their usual meanings.

For Gaussian lineshapes, the theoretical full width at half-height (FWHH) (Hz) is calculated from the second moment according to[27]

$$\Delta = (M_2 \cdot 8 \ln 2)^{1/2}/2\pi \qquad (2)$$

Due to the T_d point symmetry of the phosphate group in HT-Na_3PO_4 the ^{31}P chemical shift anisotropy will not affect the linewidth. In LT-Na_3PO_4 and in the solid solutions, however, a small contribution may be expected because the cubic local symmetry is broken in these materials.[28] As Na diffusion is thermally activated, the linewidth is gradually diminished as the correlation time τ_c characterizing the cation motion becomes comparable to Δ^{-1}. For $\tau_c\Delta \ll 1$, the contribution (b) in eq 1 is completely averaged away, and the static ^{31}P lineshape is now dominated by the homonuclear contribution (a) between the stationary ^{31}P spins. From temperature-dependent studies of the ^{31}P linewidth it is possible in principle to extract microscopic dynamical parameters. While various semiempirical procedures have been used to analyze such data, depending on the situation at hand,[29,30] a simple estimate of the activation energy of the motional process can generally be obtained using the Waugh−Fedin expression[31]

$$E_a/(\mathrm{kJ\ mol^{-1}}) \approx 0.156(T_c/\mathrm{K}) \qquad (3)$$

where T_c is the onset temperature at which motional narrowing effects become noticeable in the NMR spectrum.

Influence of Sodium Motion on the ^{23}Na Spin Hamiltonian. Under rigid lattice conditions, the static ^{23}Na NMR lineshape is influenced by multiple anisotropic interactions, including second-order quadrupolar broadening, chemical shift anisotropy, and homo- and heteronuclear dipole−dipole couplings. For this reason, motional narrowing effects on the anisotropically broadened static ^{23}Na NMR spectra are difficult to analyze in terms of dynamical parameters. A more useful source of information are the ^{23}Na relaxation characteristics in a time and temperature regime where the anisotropy is averaged away (megahertz timescale). In this isotropic regime, the ^{23}Na spin dynamics are dominated by electric field gradient fluctuations, producing unique features in longitudinal and transverse relaxation rates as well as peak positions.

The theory of quadrupolar relaxation in isotropic media was developed two decades ago,[32−35] and excellent reviews are available in the literature.[36,37] For a stochastic motional process, the electric field gradient fluctuations are characterized by a spectral density $J(\omega)$:

$$J(\omega) = \frac{\pi^2}{5} C_Q^2 \left(1 + \frac{\eta^2}{3}\right) \frac{\tau_c}{1 + \omega^2 \tau_c^2} \qquad (4)$$

where C_Q and η are the nuclear electric quadrupolar coupling constant (Hz) and the asymmetry parameter characterizing the fluctuating electric field gradient. This expression is based on an exponential form of the autocorrelation function. The motional correlation time τ_c is assumed to follow an Arrhenius law temperature dependence

$$\tau_c = \tau_{co} \exp\{E_a/RT\} \qquad (5)$$

characterized by an activation energy E_a and a preexponential factor τ_{co}, the inverse of which is interpreted as the "attempt frequency" of a cation jump.

Following application of a 90° pulse the relaxation behavior of half-integer nuclei is described by a superposition of $I + 1/2$ exponentials. For $I = 3/2$, quadrupolar relaxation under these "nonextreme narrowing conditions" is biexponential, and the decay of the magnetization in an inversion recovery experiment is given analytically by[32]

$$-\frac{\langle I_z\rangle - \langle I_z(\infty)\rangle}{2\langle I_z(\infty)\rangle} = \frac{4}{5}e^{-t/T_{1a}} + \frac{1}{5}e^{-t/T_{1b}} \tag{6}$$

Thus, in the limit of slow dynamics ($\omega_o\tau_c \geq 1$) two distinct longitudinal relaxation times T_{1a} and T_{1b} can be measured, in principle, which are related to the spectral density functions as

$$1/T_{1a} = 2J_2(2\omega_0) \tag{7a}$$

and

$$1/T_{1b} = 2J_1(\omega_0) \tag{7b}$$

As the temperature increases, these relaxation times become more similar to each other, resulting in monoexponential relaxation behavior in the *extreme narrowing limit* $\omega_o\tau_c \ll 1$:

$$\frac{1}{T_1} = \frac{2\pi^2}{5}C_Q^{\ 2}\left(1 + \frac{\eta^2}{3}\right)\tau_c \tag{8}$$

Even outside this limit, the biexponential magnetization recovery according to eq 6 is frequently not resolved by the experimental data, and only a single effective relaxation time T_1 is measured.[38,39] In this case, the well-known expression derived by Bloembergen, Purcell, and Pound[40] remains a satisfactory approximation.[17,41]

Biexponential behavior outside the extreme narrowing regime is more easily seen in the experimental free induction decays, which contain information about transverse relaxation times T_2 and second-order dynamic frequency shifts $\omega_c^{(2)}(\tau_c)$.[33−35] The theory of quadrupolar relaxation predicts

$$\frac{\langle I_x\rangle + i\langle I_y\rangle}{i\langle I_z\rangle} = \frac{2}{5}e^{-i(\omega_o + \omega_c^{(2)}(\tau_c))t}e^{-t/T_{2c}} + \frac{3}{5}e^{-i(\omega_o + \omega_s^{(2)}(\tau_c))t}e^{-t/T_{2s}} \tag{9}$$

The relaxation rates $1/T_{2c}$ and $1/T_{2s}$ arise from the central $|+1/2\rangle \leftrightarrow |-1/2\rangle$ and the $|\pm1/2\rangle \leftrightarrow |\pm3/2\rangle$ satellite transitions, respectively, and are given by

$$1/T_{2c} = J_1(\omega_o) + J_2(2\omega_o) \tag{10a}$$

$$1/T_{2s} = J_0(0) + J_1(\omega_o) \tag{10b}$$

Following Fourier transformation of the free induction decay, two distinct lineshape components are observed, with full widths at half-height

$$\Delta_c = 1/\pi T_{2c} \tag{11a}$$

$$\Delta_s = 1/\pi T_{2s} \tag{11b}$$

The sharper component, which contributes 40% to the total integrated intensity, arises from the central transition, and the broader component, which contributes 60%, comprises the satellite transitions. Equation 10b (in conjunction with eq 4) predicts a steep increase of the satellite transition linewidth with decreasing temperature, whereas eq 10a states that the linewidth of the central transition in the nonextreme narrowing limit initially increases with decreasing temperature, goes through a maximum at the temperature where $\omega_o\tau_c = 1$, and decreases again as the temperature is lowered further. Finally, eq 9 implies that the centroids of the two lineshape components do not coincide. Rather, their positions are affected by the second-order dynamic frequency shifts:[33−36]

$$\omega_c^{\ (2)} = Q_2(2\omega_o) - Q_1(\omega_o) \tag{12a}$$

$$\omega_s^{\ (2)} = Q_1(\omega_o) \tag{12b}$$

Here, $Q(\omega)$ is the imaginary component of the spectral density given by

$$Q(\omega) = \frac{\pi^2}{5}C_Q^{\ 2}\left(1 + \frac{\eta^2}{3}\right)\frac{\omega\tau_c^{\ 2}}{1 + \omega^2\tau_c^{\ 2}} \tag{13}$$

Altogether, the ^{31}P NMR linewidths, as well as the temperature and frequency dependences of the longitudinal and transverse relaxation rates and the dynamic frequency shifts present independent spectroscopic parameters, allowing the sodium diffusion to be characterized on various distinct experimental timescales.

Experimental Section

Sample Preparation and Characterization. Powder samples of pure Na_3PO_4 were obtained by solid-state reaction of Na_2CO_3 and $Na_4P_2O_7$.[23] The solid solutions were prepared from the calculated amounts of Na_3PO_4 and Na_2SO_4, pressed to pellets, and sintered in aluminium oxide crucibles at 1200 °C. To achieve homogeneity, the pellets had to be reground once before being heated a second time. The total sintering time was up to 72 h. Sample purity was confirmed by X-ray diffraction, using a Phillips PW 1050 diffractometer with a Cu K_α source. The scanning rate was 0.06 deg/min over a 2θ range of 9−90°. Differential scanning calorimetry (DSC) was conducted with a Netzsch DSC-200 differential scanning calorimeter, using heating rates of 10 K/min. Heat treatment during the DSC or NMR measurements did not result in any phase separation effects.

NMR Studies. For structural characterization ^{31}P magic-angle spinning (MAS) NMR experiments were conducted at 121.49 MHz using a Bruker CXP-300 spectrometer upgraded with a TECMAG data acquisition system. Typical 90° pulse lengths and relaxation delays were 6 μs and 200 s, respectively. ^{23}Na MAS and multiple-quantum (MQ)-MAS NMR spectra were obtained on a Bruker DSX-500 NMR spectrometer. The ^{31}P and ^{23}Na MAS NMR spectra were recorded at typical spinning frequencies of 7 kHz, using commercial multinuclear Bruker probes with a stator diameter of 4 mm. The MQMAS-NMR technique[42,43] was applied using the three-pulse, zero-quantum (ZQ) filtering technique.[44] The RF field amplitudes of the first two hard pulses and the third soft pulse corresponded to nutation frequencies of 100 and 12.5 kHz, respectively, for a liquid sample. The optimized pulse widths used were 3.7, 1.4, and 8.5 μS, respectively, for the three consecutive pulses. Typically, 48 scans were accmulated for each t_1 increment, at steps of 5 μs. A relaxation delay of 0.2 s was employed. Quadrature detection in the F1 dimension was achieved by the hypercomplex approach.[45] The sheared spectra were analyzed by projecting the 2-D contour plots onto the F_1 and F_2 axes.[46]

Temperature-dependent static ^{31}P NMR linewidths were measured on representative samples at 81.02 MHz, using a Bruker CXP-200 NMR spectrometer. The ^{23}Na spin−lattice relaxation times T_1 were measured at 16 and 79.4 MHz,

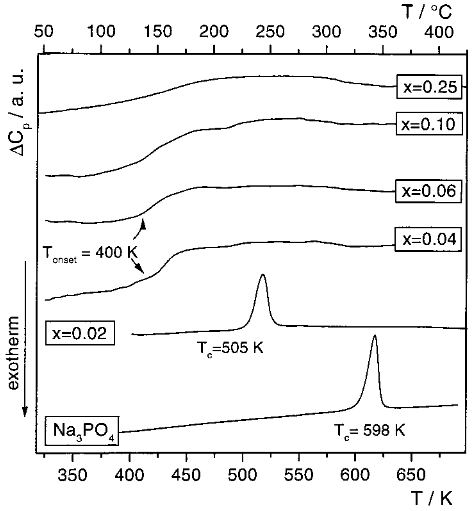

Figure 2. Differential scanning calorimetry of $(Na_3PO_4)_{1-x}-(Na_2SO_4)_x$ solid solutions.

TABLE 1: ^{31}P Isotropic Chemical Shifts and Full Widths at Half-Height Obtained from the MAS-NMR Spectra of $Na_{3-x}P_{1-x}S_xO_4$ Solid Solutions

x	0	0.04	0.10	0.25
δ/ppm[a] (±0.1)	13.8	14.1	14.3	14.3
FWHH/Hz (±10)	150	260	280	345

[a] Relative to 85% H_3PO_4.

corresponding to magnetic field strengths of 1.42 and 7.05 T, respectively. For the low-field experiments, the Bruker CXP-300 console was interfaced with an electromagnet. At both field strengths home-built solenoidal probes were used for the high-temperature experiments up to 923 K. Temperature-dependent data below ambient temperature were taken down to 128 K, using a commercial wideline probe from Bruker Instruments. Typical 90° pulse lengths ranged from 6 μs (at room temperature) to 25 μs (at 923 K), for both ^{23}Na and ^{31}P. Temperature gradients within the probes were carefully mapped out, and the effects of thermal gradients across the samples were minimized by spectroscopic measurements as a function of sample length. At representative temperatures the ^{23}Na nutation behavior was carefully characterized; conventional inversion recovery and saturation recovery pulse sequences were then used to measure the longitudinal relaxation rates.

Results, Data Analysis, and Interpretation

Differential Scanning Calorimetry. Figure 2 shows the characterization of Na_3PO_4 and its solid solutions with Na_2SO_4, by differential scanning calorimetry. Pure Na_3PO_4 shows a first-order phase transition at 598 K. The transition temperature is reduced to 505 K, if the material is doped with 2% Na_2SO_4. There is also a hysteresis of 25 K between the heating and cooling cycles. The first-order phase transition is suppressed altogether in the solid solutions having sulfate contents of 4% and higher. Materials within the compositional regions $0.04 < x < 0.10$ show a second-order phase transition with an onset temperature T_0 near 400 K, whereas the sample with $x = 0.25$ shows no clear evidence of sudden heat capacity changes. The DSC and XRD data indicate that the cubic phase is now stabilized to room temperature with structurally disordered PO_4^{3-} tetrahedra. We interpret the second-order phase transition near 400 K to be associated with an abrupt onset of dynamic disordering of the phosphate groups.

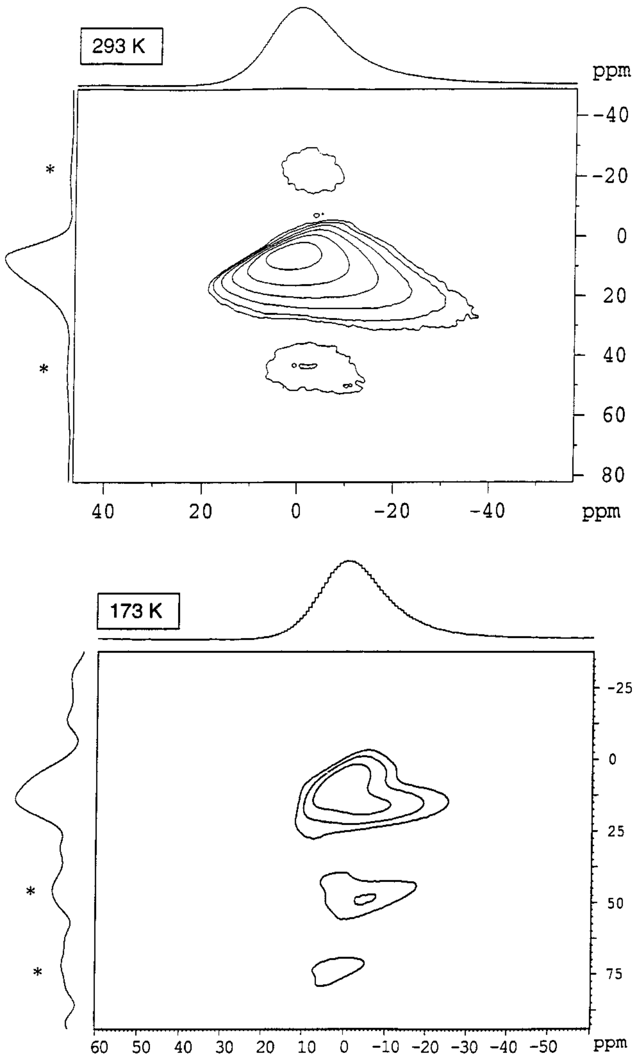

Figure 3. ^{23}Na triple-quantum MAS-NMR spectra of the solid solution $(Na_3PO_4)_{0.9}-(Na_2SO_4)_{0.1}$: top, $T = 293$ K; bottom, $T = 173$ K. Vertical and horizontal axes refer to the isotropic and anisotropic dimensions, respectively. Spinning sidebands are indicated by asterisks.

High-Resolution ^{23}Na and ^{31}P Solid-State NMR. Table 1 summarizes the results of ^{31}P magic angle spinning experiments undertaken on representative samples. Since both the tetragonal low-temperature phase and the cubic high-temperature modification of Na_3PO_4 have only a single phosphorus site, the MAS NMR spectra consist of a single line in each case. The ^{31}P isotropic chemical shift of 13.8 ppm (vs 85% H_3PO_4) observed in tetragonal Na_3PO_4 agrees well with the literature values,[47] and the transition to the HT-phase has only a minor effect on the chemical shift. Likewise, only small changes are observed in the NMR parameters of the solid solutions with Na_2SO_4. Note, however, the significantly increased MAS-NMR linewidths compared to those of HT-Na_3PO_4. This peak broadening reflects chemical shift distribution effects arising from nonuniformities in the local phosphorus environment, which can be attributed to the statistical distribution of vacancies present in the $Na_2SO_4-Na_3PO_4$ solid solutions.

^{23}Na MAS and MQMAS experiments were undertaken with the goal of differentiating between the cations occupying the tetrahedral and octahedral interstitial sites. However, at room temperature, neither HT-Na_3PO_4 nor its solid solutions with sodium sulfate give rise to spectroscopically resolvable MAS-NMR signals. Figure 3 shows MQMAS-NMR spectra obtained on $(Na_3PO_4)_{0.9}-(Na_2SO_4)_{0.1}$ at 293 and 173 K, respectively. While only an asymmetric lineshape is observable near room temperature, the low-temperature spectra do suggest some partial

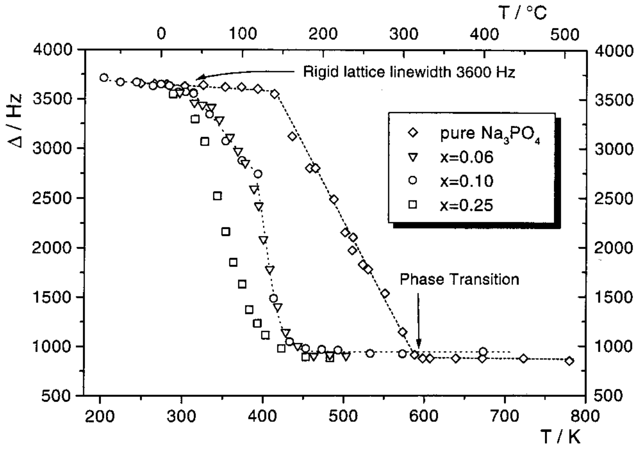

Figure 4. Temperature dependence of static ^{31}P NMR linewidths in $(Na_3PO_4)_{1-x}-(Na_2SO_4)_x$ solid solutions.

discrimination of two spectral components, although the resolution remains poor. This is not surprising, because the statically disordered PO_4^{3-} tetrahedra produce nearly continuous variations in the static electric field gradient experienced by the sodium nuclei in both sites. The situation is comparable to the line broadening effects widely observed for ^{23}Na and ^{27}Al nuclei in glasses.[48] From the field dependence of the centers of gravity of MAS spectra taken at 79.4 and 132.3 MHz at room temperature, average isotropic chemical shifts and nuclear electric quadrupolar coupling parameters can be estimated. For the $x = 0.10$ sample, a C_q' value of $C_Q(1 + \eta^2/3)^{1/2}$ equal to 2.5 ± 0.2 MHz and an isotropic chemical shift of 7 ± 1 ppm have been obtained. This result was also confirmed by the MQ-MAS data of Figure 3. Other compositions are expected to have very similar NMR parameters, because the lineshapes and positions of their MAS spectra are virtually identical.

Variable-Temperature Static ^{31}P NMR. Temperature-dependent measurements of the static ^{31}P NMR spectra show purely Gaussian shapes at temperatures below 420 K and above 573 K; in the temperature interval between, a mixture of equal Gaussian and Lorentzian fractions gives the best fit to the experimental spectra. The corresponding FWHH measured from these spectra at 81.02 MHz are displayed in Figure 4. The Gaussian rigid lattice linewidth of low-temperature Na_3PO_4 is measured to be 3600 Hz. Using eqs 1 and 2, a linewidth of 3300 Hz is calculated for LT-Na_3PO_4 from structural data in reasonably good agreement with experiment. The small discrepancy is attributed to a contribution arising from the chemical shift anisotropy, since it is known that in low-temperature sodium orthophosphate the PO_4^{3-} anions show slight deviations from their ideal tetrahedral symmetry.[28] As the temperature is increased, motional narrowing effects become clearly observable in the static ^{31}P NMR spectra: the linewidth is reduced and the spectra attain partial Lorentzian character. Finally, in the cubic phase formed above the phase transition temperature, a constant Gaussian linewidth of 850 Hz is measured. Taking into account the known internuclear ^{31}P−^{31}P distances in the crystal structure, and assuming that both the *A* and *B* terms of the dipolar Hamiltonian are relevant, a theoretical linewidth of 815 Hz is expected. This value is reached at a temperature just below the phase transition, indicating that already in LT-Na_3PO_4 the cation motion is thermally activated on the millisecond timescale, modulating the heteronuclear ^{23}Na−^{31}P dipole−dipole interactions within the temperature range $450 \text{ K} < T < 600 \text{ K}$. In the plastic crystalline state above the phase transition, no residual ^{31}P−^{23}Na heterodipolar contribution remains, indicating that sodium motion occurs fast on the kilohertz timescale.

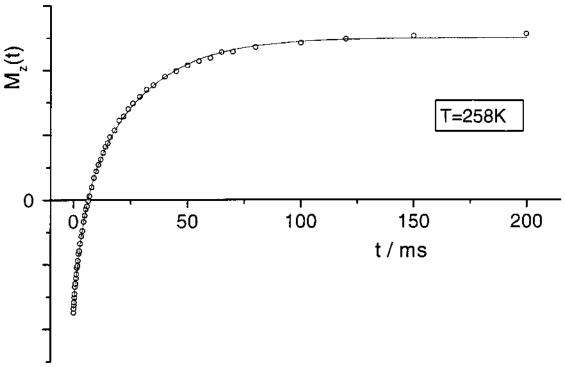

Figure 5. Magnetization recovery of $(Na_3PO_4)_{0.9}-(Na_2SO_4)_{0.1}$ solid solution measured at 258 K. The solid curve corresponds to a biexponential fit to eq 14, using $a = 0.324 \pm 0.05$, $T_{1a} = 3.89 \pm 0.2$ ms, and $T_{1b} = 25.9 \pm 0.8$ ms.

The temperature-dependent static ^{31}P NMR linewidths of the solid solutions $x = 0.06$, 0.10, and 0.25 are included in Figure 4. For $x = 0.06$ and 0.10, two clear temperature regimes can be differentiated. Within the temperature region $300 \text{ K} < T < 400 \text{ K}$, i.e., just below the onset temperature T_o of the second-order phase transition, the linewidth decreases gradually with increasing temperature. From eq 3 one can estimate an activation energy of 0.48 eV. At a temperature near T_o, however ($T > 400$ K), the linewidth falls rapidly to a constant value of 940 Hz. This value is again consistent with complete averaging of the ^{23}Na−^{31}P heteronuclear dipole−dipole coupling due to fast motion of the Na^+ ions on the kilohertz timescale. The slight discrepancy of the residual linewidth in comparison to the van Vleck value can be rationalized on the basis of chemical shift distribution effects. As discussed above, these distribution effects are also evident in the ^{31}P MAS-NMR results. Similar results are observed for the $x = 0.25$ sample, except that here the distinction between the two temperature regimes of motional narrowing is lost. This observation correlates with the DSC results, which indicate that the second-order phase transition is smeared out over a wider temperature range in this sample.

The present results illustrate that the ^{31}P static linewidth can serve as a sensitive measure of cation dynamics in this system. As discussed below in more detail, the sudden acceleration of Na^+ motion at the onset temperature of the second-order phase transition suggests that the reorientational motion of the phosphate tetrahedra and the translational motion of the sodium cations are dynamically correlated.

^{23}Na Longitudinal Relaxation: Low-Temperature Regime. In correspondence with the ^{31}P static linewidth data, the variable-temperature ^{23}Na longitudinal relaxation measurements reveal the presence of two distinct temperature regimes: In LT-Na_3PO_4 and in the $Na_3PO_4-Na_2SO_4$ solid solutions at temperatures $T < 450$ K residual anisotropic lineshape contributions are apparent, and eqs 6−8 are not applicable. 2-D nutation NMR[49] experiments (data not shown) confirm that at these temperatures only the central $|1/2\rangle \leftrightarrow |-1/2\rangle$ coherence is affected by the pulse sequence. In the present study, we report results obtained for two solid solution samples corresponding to $x = 0.06$ and 0.1, respectively. As Figure 5 indicates, the magnetization recovery can be approximated by a biexponential fit to two characteristic relaxation times T_{1a} and T_{1b} according to the formula

$$-\frac{\langle I_z\rangle - \langle I_z(\infty)\rangle}{\langle I_z(\infty)\rangle} = \{(1-a)e^{-t/T_{1a}} + a\cdot e^{-t/T_{1b}}\}\cdot\epsilon \qquad (14)$$

In eq 14, $\epsilon = 1$ and $\epsilon = 2$ for saturation and inversion recovery experiments, respectively. Satisfactory biexponential

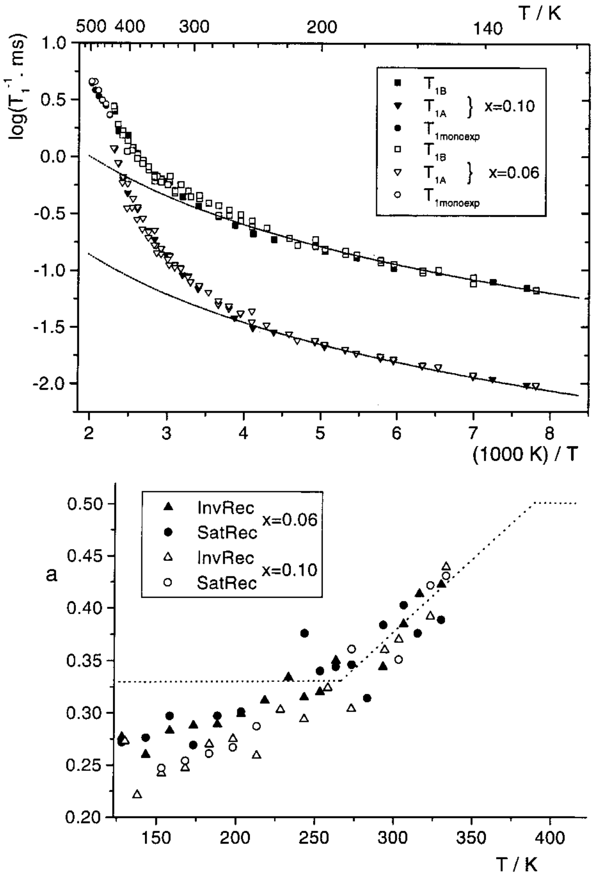

Figure 6. (a, top) Temperature dependence of the biexponential relaxation rates T_{1a}^{-1} and T_{1b}^{-1} at 79.4 MHz in two $(Na_3PO_4)_{1-x}-(Na_2SO_4)_x$ solid solutions ($x = 0.06$ and 0.10). Solid curves correspond to a phenomenological fit to parabolic functions $T_1^{-1} = \beta T^2$. (b, bottom) Temperature dependence of the fit parameter *a* in eq 14. The dashed horizontal lines denote the theoretical limit $a = 0.5$ expected in the case of selective excitation of the central transitions of ^{23}Na spins rapidly exchanging between the tetrahedral and the octahedral interstitial sites at high temperatures, and the theoretical limit $a = 0.33$ expected in the case of T_1 differentiation between these two sites at low temperature (2:1 ratio). For further discussion see the text.

fits were obtained for all of the data measured within the temperature range 128 K $< T <$ 433 K. Near the high-temperature end of this regime, *a* values in the vicinity of 0.5 are observed, consistent with selective excitation of the central coherence.[50] Figure 6a summarizes the temperature dependences of the two relaxation rates in this low-temperature limit for two solid solution samples with $x = 0.06$ and 0.10. Significantly, however, the biexponential fitting parameter *a* decreases systematically with decreasing temperature, down to values of 0.25−0.3 at low temperatures (see Figure 6b). This behavior is not expected for uniformly relaxing Na$^+$ species in the selective excitation limit. Along with the apparent decrease in *a*, the relaxation measurements indicate systematic lineshape changes as a function of inversion recovery time. As shown in Figure 7a, these experiments allow a deconvolution of the ^{23}Na MAS-NMR spectra into a narrow component with a shorter T_1 and a broader component with a longer T_1. The ratio of these two components is close to the 1:2 ratio of octahedral and tetrahedral interstitial sites present in the sample. Excellent agreement with the experimental result is observed by assigning the broader contribution to the tetrahedral sites, whereas the reverse assignment does not produce satisfactory agreement (Figure 7b). These results suggest that at lower temperatures the relaxation times of these two sites are differentiable and not equalized by site exchange or spin diffusion. Keeping in mind the theoretical prediction of biexponential behavior for each sodium site, in this dynamical regime the magnetization recovery curves are actually expected to contain four distinct contributions. Nevertheless, eq 14 accounts well for the data, and the precision is insufficient to justify any increase in the number of fitting parameters. As Figure 6a indicates further, the T_1 curves are independent of the composition parameter *x*, and no frequency dependence is observed. In the low-temperature limit the data can be approximated by a T^2 law as predicted for relaxation due to phonon coupling.[51] On the basis of these results, we conclude that the ^{23}Na T_1 values in this low-temperature regime are insensitive to cation diffusion or to the motion of the phosphate ions, presumably because the motion proceeds two slow compared to the NMR timescale (10^{-6} s) relevant here.

^{23}Na Longitudinal Relaxation: High-Temperature Regime. Figure 8 shows the temperature dependence of the longitudinal relaxation rate at 79.4 MHz for pure HT-Na_3PO_4 and for the solid solutions containing 2−25% Na_2SO_4 at temperatures $T >$ 450 K where approximately monoexponential recovery is observed. In all of the solid solution phases these $\log(T_1^{-1})$ vs. 10^3T^{-1} curves give evidence of two distinct contributions (and hence motional processes): one relaxation rate maximum occurs uniformly at temperatures near 500 K (process 1). The sulfate dopant concentration appears to have only a minor influence on the position of this maximum, and the T_1 values (0.2 ms) at the corresponding temperatures are compositionally invariant within the limits of experimental error. A second relaxation rate maximum is observed at higher temperatures, and the importance of this mechanism increases with increasing dopant concentration (process 2).

Parts a−c of Figure 9 show the corresponding theoretical analysis of temperature- and frequency-dependent data sets obtained on solid solutions containing 4 and 10 mol % Na_2SO_4, and on pure HT-Na_3PO_4, respectively. By approximating the decay as monoexponential, it was possible to fit these relaxation curves as a superposition of two individual contributions, corresponding to processes 1 and 2, respectively:

$$T_1^{-1} = C_1\left\{\frac{\tau_{c1}}{1+\omega_0^2\tau_{c1}^2} + \frac{4\tau_{c1}}{1+4\omega_0^2\tau_{c1}^2}\right\} + C_2\left\{\frac{\tau_{c2}}{1+\omega_0^2\tau_2^2} + \frac{4\tau_{c2}}{1+4\omega_0^2\tau_{c2}^2}\right\} \quad (15)$$

In eq 15, standard BPP theory was assumed to be applicable for each contribution. The corresponding relaxation strengths C_1 and C_2 are given by

$$C_i = \frac{2\pi^2}{25}C_Q^2\left(1+\frac{\eta^2}{3}\right)f(x)\kappa \quad (16)$$

For both processes, the adjustable parameter κ (which is on the order of unity) takes into account possible peculiarities in the ionic motion that differ from the premises made in BPP theory. Furthermore, the factor $f(x)$ allows for the fact that the importance of this relaxation mechanism may depend on the sulfate dopant concentration.[52] As Figure 9a,b illustrates further, the above dual BPP analysis with the fit parameters listed in Table 2 also succeeds in fitting the temperature dependence of $T_{1\rho}$—data obtained at a Larmor frequency of 79.4 MHz and an apparent rotating frame frequency of $\nu_1 = 20$ kHz to the appropriate theoretical expressions.[19] (These $T_{1\rho}$ measure-

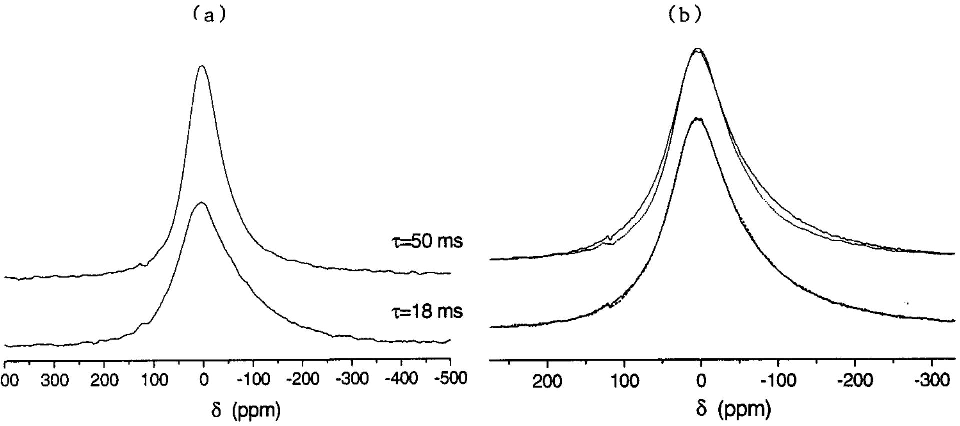

Figure 7. (a) ^{23}Na spectral editing via inversion recovery in $(Na_3PO_4)_{0.9}-(Na_2SO_4)_{0.1}$ solid solution, measured by MAS at 127 K. The τ value denotes the delay between the inversion and the detection pulses. The spectrum with $\tau = 18$ ms has been subjected to a 180° phase correction; thus the broader component is characterized by the longer T_1. (b) Comparison of the experimental ^{23}Na MAS NMR spectrum at 127 K with a simulation assuming intensity ratios broad:narrow of 1:2 (top) and 2:1 (bottom), respectively. The better agreement of the bottom spectrum with the simulation suggests that the broad component must be assigned to the sodium ions occupying the tetrahedral interstitial sites.

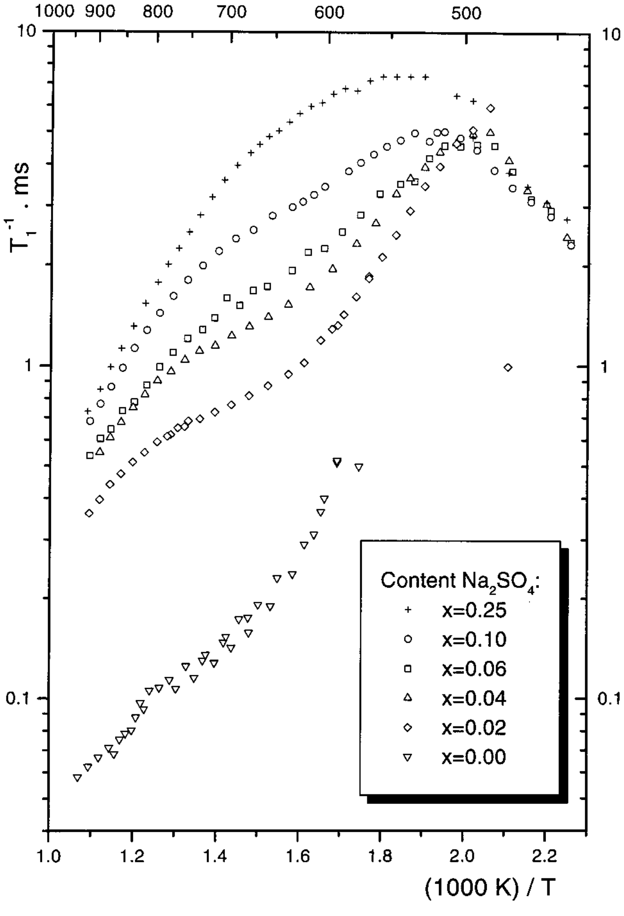

Figure 8. Temperature dependence of the 79.4 MHz ^{23}Na longitudinal relaxation rates in $(Na_3PO_4)_{1-x}-(Na_2SO_4)_x$ solid solutions.

ments were restricted to the high-temperature region where monoexponential decays were observed).

In the relaxation analysis of pure HT-Na_3PO_4, process 2 makes only a minimal (albeit detectable) contribution. The longitudinal relaxation is dominated by process 1, although the phase transition intervenes at 598 K before the corresponding rate maximum is reached. Table 2 summarizes the fitting parameters obtained for all of the samples. Comparison of the best-fit C_1 values with the calculated value (using the known C_q' from low-temperature MAS lineshape analysis, see above) indicates that the correction factors κ lie in the vicinity of 0.4.

Temperature-Dependent ^{23}Na NMR Transverse Relaxation and Lineshape. In all of the solid solution samples, the ^{23}Na NMR lineshapes are purely Lorentzian at temperatures above 800 K as expected for the *extreme narrowing limit*. As the temperature is lowered, the expected bi-Lorentzian lineshape predicted from eqs 10a and 10b appears (see Figure 10). In parts a−c of Figure 11, the temperature-dependent FWHHs of both components are contrasted with calculated values (eqs 10 and 11 in conjunction with eq 4) for the samples $x = 0.25$, 0.10, and 0.06, respectively. Both relaxation processes 1 and 2 have been taken into account using the same dynamical parameters as those extracted from the ^{23}Na-T_1 data described in the previous section:

$$\Delta_c = \frac{1}{T_{2c}\pi} = \frac{5}{2\pi}\left[C_1\left\{\frac{\tau_{c1}}{1+\omega_0^2\tau_{c1}^2} + \frac{\tau_{c1}}{1+4\omega_0^2\tau_{c1}^2}\right\} + C_2\left\{\frac{\tau_{c2}}{1+\omega_0^2\tau_{c2}^2} + \frac{\tau_{c2}}{1+4\omega_0^2\tau_{c2}^2}\right\}\right]$$

$$\Delta_s = \frac{1}{T_{2s}\pi} = \frac{5}{2\pi}\left[C_1\left\{\tau_{c1} + \frac{\tau_{c1}}{1+\omega_0^2\tau_{c1}^2}\right\} + C_2\left\{\tau_{c2} + \frac{\tau_{c2}}{1+\omega_0^2\tau_{c2}^2}\right\}\right] \quad (17)$$

For Δ_c in particular, excellent fits to eq 17 are obtained. Refined best-fit values are summarized in Table 3. Moving away from the extreme narrowing limit with decreasing temperature, the linewidths are first dominated by process 2, whereas toward lower temperatures process 1 becomes increasingly important. At temperatures below 430 K the experimental linewidths diverge from the theoretically predicted ones. These discrepancies reflect anisotropic contributions to the ^{23}Na NMR central transition lineshapes that are no longer accounted for by the theory of isotropic quadrupolar relaxation. Significantly this occurs at temperatures close to the second-order phase transition, where both the ^{23}Na and ^{31}P static linewidths increase steeply by several kilohertz over a very narrow temperature range. As the temperature is lowered further, a gradual approach to the limiting rigid lattice values is observed for both nuclear species.

Inspection of Figure 11 also reveals that the agreement between the experimental and the theoretically expected linewidths Δ_s of the broader satellite component is significantly

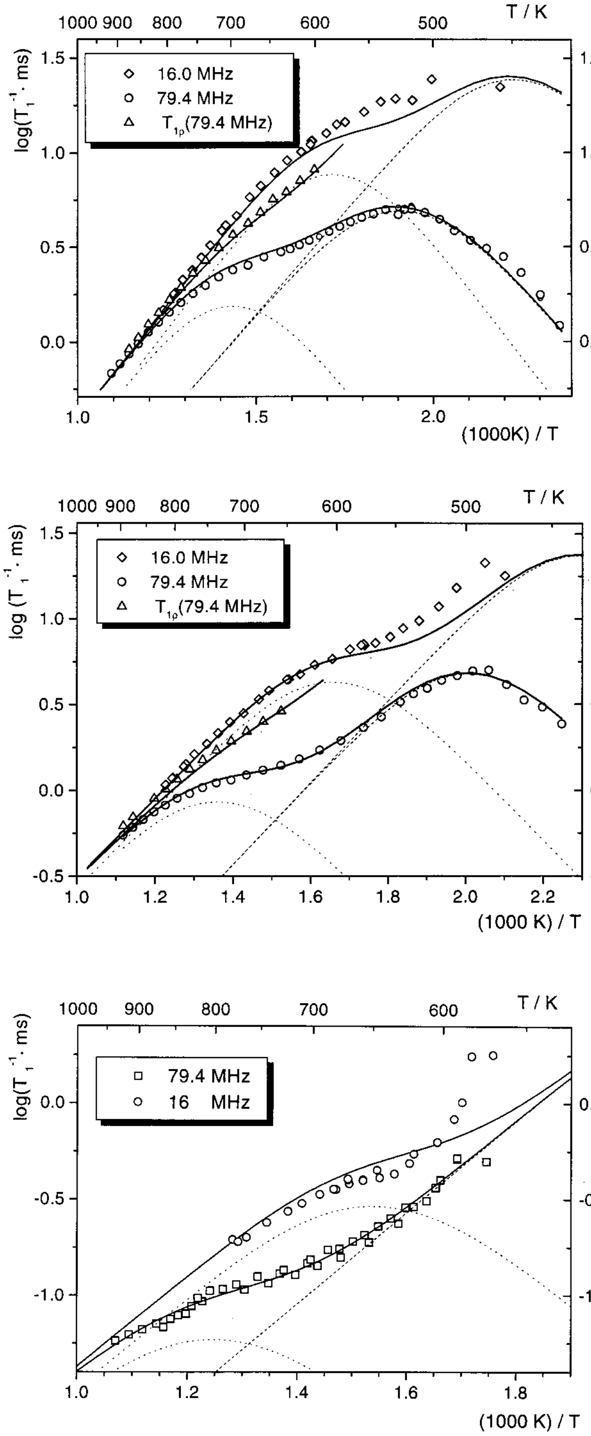

Figure 9. Temperature and frequency dependence of the ^{23}Na longitudinal relaxation rates in $(Na_3PO_4)_{1-x}-(Na_2SO_4)_x$ solid solutions. Dashed, dotted, and solid curves denote the fitted contributions of processes 1 and 2, and their superposition, respectively. Longitudinal relaxation rates in the rotating frame measured over a limited temperature range are also included. (a, top) $(Na_3PO_4)_{0.9}-(Na_2SO_4)_{0.1}$ solid solution. (b, middle) $(Na_3PO_4)_{0.96}-(Na_2SO_4)_{0.04}$ solid solution. (c, bottom) HT-Na_3PO_4.

TABLE 2: Fit Parameters Used for Analysis of the T_1 Data in $(Na_3PO_4)_{1-x}-(Na_2SO_4)_x$ Solid Solutions

		0.00	0.02	0.04	0.06	0.10	0.25
process 1	$C^{(1)}/10^{12}\ s^{-2}$	1.6	2.0	1.7	1.7	1.7	2.1
	$\tau_{c0}^{(1)}$/ps	0.005	0.011	0.02	0.023	0.09	0.09
	$E_A^{(1)}$/eV	0.47	0.47	0.47	0.47	0.43	0.43
process 2	$C^{(2)}/10^{12}\ s^{-2}$	0.02	0.18	0.30	0.41	0.54	1.2
	$\tau_{c0}^{(2)}$/ps	1.3	1.7	0.8	0.8	0.35	0.25
	$E_A^{(2)}$/eV	0.47	0.43	0.47	0.45	0.49	0.46

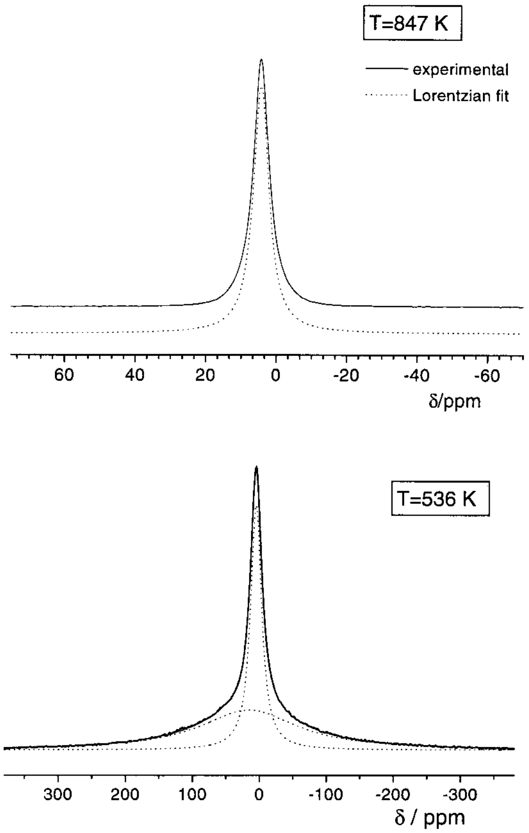

Figure 10. ^{23}Na NMR lineshape in $(Na_3PO_4)_{0.94}-(Na_2SO_4)_{0.06}$ solid solutions at 536 and 847 K, respectively. Dotted curves denote Lorentzian or bi-Lorentzian fits to the experimental lineshape.

worse than for the sharper central transitions: this is particularly true at the lower temperatures. Increasing the activation energy of process 2 (which dominates this quantity) by 25% would result in a satisfactory match, but this would also produce a poorer fit to the linewidth data for the sharp component. Since the lineshape parameters for the broad satellite components are generally determined with lower precision than those for the sharp central components, we attach less significance to this discrepancy. Furthermore, it is quite possible that in this temperature regime the satellite linewidths are still affected by residual anisotropic broadening due to static first-order quadrupolar interactions, producing an excess width.

The temperature-dependent evolution of the ^{23}Na NMR lineshape in pure HT-sodium orthophosphate is rather distinct from that of all of the solid solutions. At temperatures above 850 K, a single Lorentzian lineshape is observed, indicating the approach to the extreme narrowing condition. At lower temperatures, however, the spectrum consists of a narrow component and a broad component, neither of which possesses Lorentzian shape (an example is given in Figure 12). Satisfactory linefits can only be achieved if a partial Gaussian character of each component is allowed. We believe that, due to a reduced dimensionality of the cation motion in this material, these lineshapes are still influenced by anisotropic contributions (dipolar and quadrupolar) to the ^{23}Na spin Hamiltonian. A more detailed discussion of these effects will be presented in a separate paper devoted to the cation and anion dynamics in HT-Na_3PO_4.

^{23}Na Dynamic Frequency Shifts. Parts a–c of Figure 13 show the temperature dependences of the ^{23}Na resonance shifts

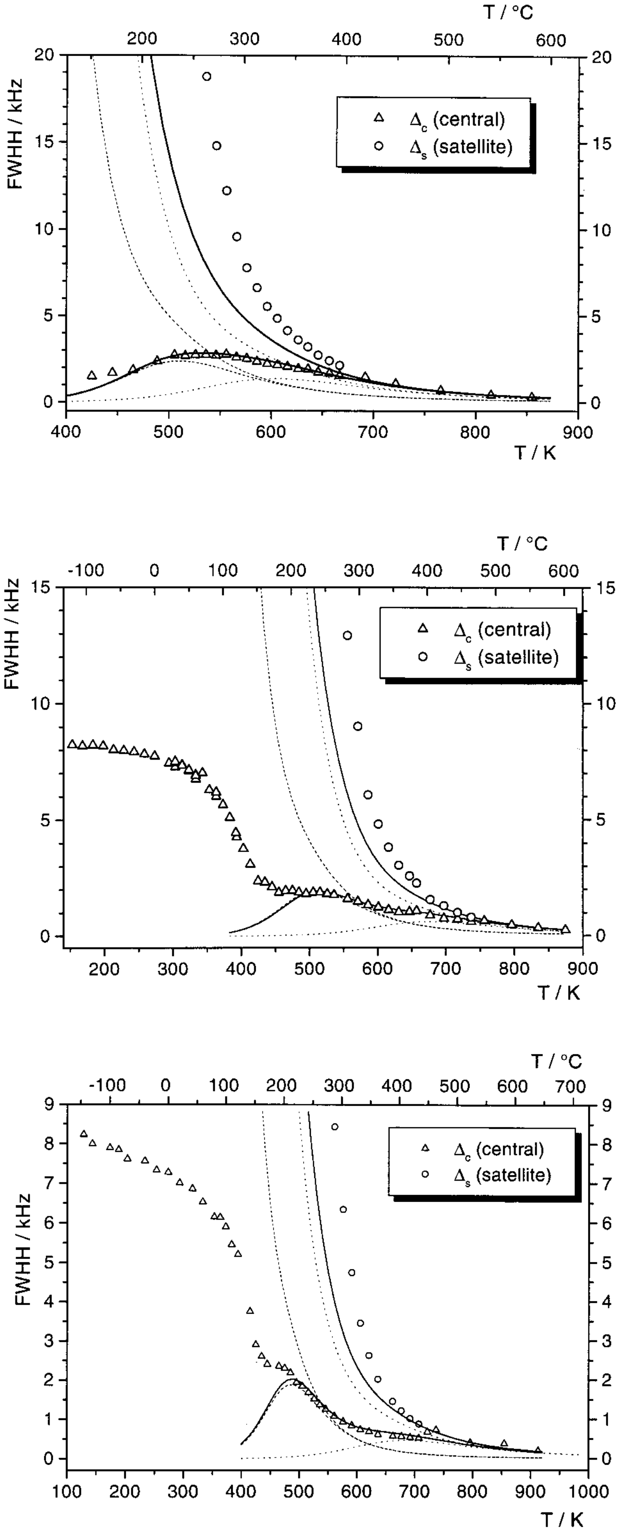

Figure 11. Temperature dependence of the ^{23}Na central and satellite transition linewidths in $(Na_3PO_4)_{1-x}-(Na_2SO_4)_x$ solid solutions. Dashed, dotted, and solid curves denote the fitted contributions of processes 1 and 2, and their superposition, respectively. (a, top) $(Na_3PO_4)_{0.75}-(Na_2SO_4)_{0.25}$ solid solution. (b, middle) $(Na_3PO_4)_{0.9}-(Na_2SO_4)_{0.1}$ solid solution. (c, bottom) $(Na_3PO_4)_{0.94}-(Na_2SO_4)_{0.06}$ solid solution.

TABLE 3: Fit Parameters Used for the Analysis of Central Transition Linewidths and Dynamic Frequency Shifts (in Parentheses) in $(Na_3PO_4)_{1-x}-(Na_2SO_4)_x$ Solid Solutions

		0.02	0.04	0.06	0.10	0.25
process 1	$C^{(1)}/10^{12}$ s^{-2}	2.0 (1.8)	1.8 (1.8)	1.7 (1.8)	1.6 (1.7)	2.0 (1.7)
	$\tau_{c0}^{(1)}$/ps	0.011 (0.020)	0.020 (0.023)	0.023 (0.023)	0.09 (0.09)	0.09 (0.09)
	$E_A^{(1)}$/eV	0.47	0.47	0.47	0.43	0.43
process 2	$C^{(2)}/10^{12}$ s^{-2}	0.18 (0.18)	0.28 (0.27)	0.39 (0.37)	0.52 (0.54)	1.14 (1.20)
	$\tau_{c0}^{(2)}$/ps	1.70 (1.70)	0.88 (0.85)	0.80 (0.80)	0.35 (0.35)	0.25 (0.25)
	$E_A^{(2)}$/eV	0.43	0.47	0.45	0.49	0.46

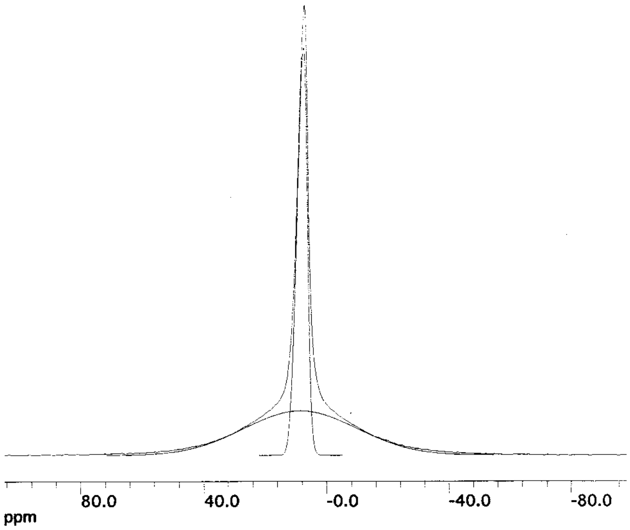

Figure 12. Static ^{23}Na NMR spectrum of HT-Na_3PO_4, measured at 79.4 MHz and 791 K. Underlying curves indicate the fitting components of two lineshape contributions having mixed Gaussian/Lorentzian character.

δ_c and δ_s (narrow and broad components) of the solid solution samples $x = 0.25$, 0.10, and 0.06. At high temperatures, where extreme narrowing conditions obtain, the shifts are temperature invariant, with values ranging from 6.5 to 4.5 ppm vs. 1 M NaCl solution for all compositions. Below 720 K, however, the predictions of eq 12 for relaxation in the nonextreme narrowing limit are realized. The centers of the narrow and broad Lorentzian contributions of the lineshape displayed in Figure 10 do not coincide, resulting in an asymmetric appearance of the overall spectra.

To obtain appropriate phasing, the DISPA method[34] introduced by Werbelow and co-workers was used, where the amplitude of the dispersion signal is plotted versus that of the absorption signal. Perfect Lorentzian lineshapes are represented by a circle, whose center is rotated about the origin by phasemisadjustments. In the case of two noncoincident but partially overlapping Lorentzians of different widths, a characteristic deviation of the DISPA plot from this reference circle is observed. The phase was adjusted by minimizing the rotation of the DISPA plot, and then the NMR line was fitted. An example is illustrated in Figure 14, representing the data of Figure 10, bottom. In Figure 13 the high frequency shifts pertain to the broad component, which escapes detection at temperatures $T < 480$ K. The low-frequency shifts pertain to the narrow component. Uncertainties are given by ±2% of the width of each component. The error is larger again in the temperature range where central and satellite components have comparable widths. The solid line represents the theoretical dependence of the resonance shift, taking both processes 1 and 2 into account:

$$\delta_c = \delta' + \delta_c^{(2)} \text{ and } \delta_s = \delta' + \delta_s^{(2)}$$

$$\delta_c^{(2)} = 5\frac{1}{2\pi\nu_0}\left[C_1\left\{\frac{2\omega_o\tau_{c1}^{\,2}}{1 + 4\omega_o^{\,2}\tau_{c1}^{\,2}} - \frac{\omega_o\tau_{c1}^{\,2}}{1 + \omega_o^{\,2}\tau_{c1}^{\,2}}\right\} + C_2\left\{\frac{2\omega_o\tau_{c2}^{\,2}}{1 + 4\omega_o^{\,2}\tau_{c2}^{\,2}} - \frac{\omega_o\tau_{c2}^{\,2}}{\omega_o^{\,2}\tau_{c2}^{\,2}}\right\}\right] \tag{18a}$$

$$\delta_s^{(2)} = 5\frac{1}{2\pi\nu_0}\left[C_1\frac{\omega_o\tau_{c1}^{\,2}}{1 + \omega_o^{\,2}\tau_{c1}^{\,2}} + C_2\frac{\omega_o\tau_{c2}^{\,2}}{1 + \omega_o^{\,2}\tau_{c2}^{\,2}}\right] \tag{18b}$$

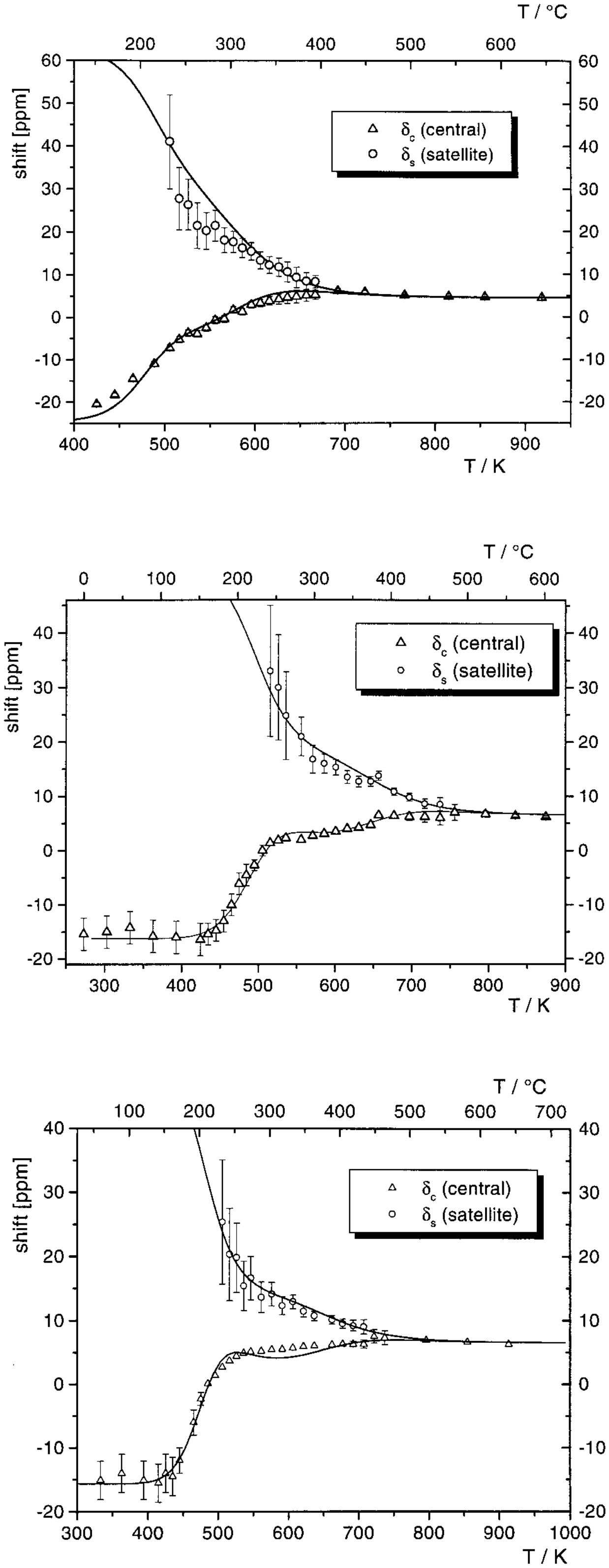

Figure 13. Temperature dependence of the ^{23}Na resonance shifts δ_c and δ_s pertaining to the central and satellite transitions, respectively, in $(Na_3PO_4)_{1-x}$–$(Na_2SO_4)_x$ solid solutions. Solid curves denote the superposition of the fitted individual contributions (not shown) of processes 1 and 2, respectively. (a, top) $(Na_3PO_4)_{0.75}$–$(Na_2SO_4)_{0.25}$ solid solution. (b, middle) $(Na_3PO_4)_{0.9}$–$(Na_2SO_4)_{0.1}$ solid solution. (c, bottom) $(Na_3PO_4)_{0.94}$–$(Na_2SO_4)_{0.06}$ solid solution.

Here, $\delta_c^{(2)}$ and $\delta_s^{(2)}$ are the second-order dynamic frequency shifts of central and satellite components, respectively, calculated from eqs 12 and 13, while δ' is the chemical shift that is

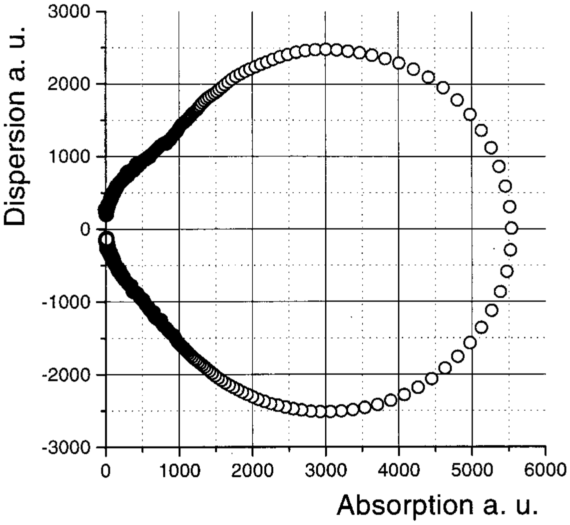

Figure 14. DISPA analysis of a 79.4 MHz spectrum of $(Na_3PO_4)_{0.94}$–$(Na_2SO_4)_{0.06}$ solid solution measured at 536 K (spectrum of Figure 10, bottom). See the text for further discussion.

independent of dynamics. For the simulation, activation energies and correlation times obtained from the fitted T_1 curves were used, with only slight adjustments in some cases. The best fit values are also included in Table 3 (given in parentheses).

Discussion and Conclusions

The results of the present study illustrate the power of complementary solid-state NMR experiments for characterizing the dynamical characteristics of sodium motion in plastic crystalline HT-Na_3PO_4 and its solid solutions with Na_2SO_4 on the basis of ^{23}Na longitudinal relaxation rates, linewidths, and peak positions. The temperature dependences of these NMR parameters can be analyzed consistently within the framework of quadrupolar relaxation theory in the nonextreme narrowing limit of isotropic systems. Previous applications of this theory have focused on the liquid state, and included the dynamical characterization of highly viscous solutions,[53,54] aqueous solutions of metal–protein complexes,[55–58] colloidal suspensions,[59] and other systems of biological relevance.[54,60–63] In the 1980s, Bjorkstam and Villa[64–67] and independently Becker[50] pointed out that transverse relaxation behavior and dynamic frequency shifts of quadrupolar nuclei should also be applicable in principle for probing ion dynamics in the solid state. Experimental data on Na–β-alumina have been discussed in this context.[64–67] The typical spectroscopic appearance of quadrupolar relaxation behavior in the nonextreme narrowing limit, including line-broadening minima and dynamic frequency shifts, has been observed previously in various other systems, including solid electrolytes[66–70] and glass-forming melts.[70,71] However, to the best of our knowledge, the present study represents the first application of isotropic quadrupolar relaxation spectroscopy to the quantitative study of ionic motion in inorganic solids.

Figure 15 summarizes the results obtained from this analysis for the $(Na_3PO_4)_{1-x}$–$(Na_2SO_4)_x$ solid solutions. Two distinct processes are identified, whose activation energies are similar and agree well with the values obtained by electrical conductivity (0.43 ± 0.02 eV for pure Na_3PO_4 and slightly less for the solid solutions). Process 2 is almost absent in pure HT-Na_3PO_4, and its relaxation strength increases significantly with increasing sulfate concentration. Along with this trend, the temperature at which the relaxation maximum is observed decreases, indicating that the process becomes faster.

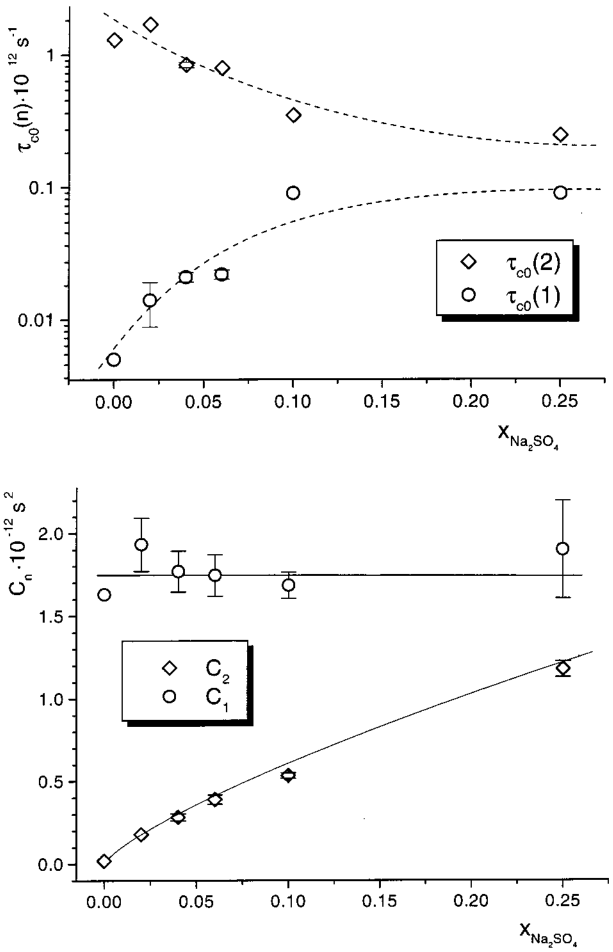

Figure 15. Compositional dependence of the dynamical parameter $\tau_{c0}(n)$ and the relaxation strengths C_n for processes n = 1 and 2, respectively, in $(Na_3PO_4)_{1-x}$–$(Na_2SO_4)_x$ solid solutions. Average values from Tables 2 and 3 are used. The error bars arise from the range of values listed there for each composition. Solid curves are guides to the eye.

On the basis of this compositional dependence, we assign process 2 to a conventional ionic hopping mechanism, which is more or less independent of the anionic motion but favored with increasing x because the substitution of PO_4^{3-} by SO_4^{2-} ions progressively generates vacancies in the cationic sublattice. At room temperature, the inversion recovery experiments reveal no distinguishable ^{23}Na MAS lineshape components, indicating that the sodium cations exchange quickly between the octahedral and tetrahedral interstitial sites. Further, the X-ray diffraction data of these solid solutions support a structural model with vacancies distributed equally over both types of sites.[23]

The relaxation process 1 is attributed to the correlated rotational motion of the PO_4^{3-} anions and the translational motion of the sodium cations. As expected, the coupling parameter C_1 is essentially invariant over the investigated compositional range. The process is triggered and accelerated by the second-order phase transition near 400 K, results in complete averaging of the ^{23}Na–^{31}P heterodipolar coupling at $T > T_o$, and further modulates the quadrupolar interactions so that the ^{23}Na central line is narrowed by a factor of 3–4 within a small temperature range. It is not possible from the NMR data to decide if one type of Na site is more involved in this correlated mechanism than the other. A previous publication supports the particular role of octahedral sodium ions in this mechanism, based on a consistent interpretation of frequency-dependent conductivity, neutron scattering, and Carr–Parinello molecular dynamics simulations.[14] Since a particularly short and strong O−Na_{oct} bond is realized in the cubic structure, this interpretation is plausible.

At temperatures $T < T_o$, the experimental data still indicate partial averaging of anisotropic interactions in the ^{31}P and ^{23}Na lineshapes over a considerable temperature range. On the basis of complementary data from ^{17}O NMR (to be published separately)[72] it appears likely that here both vacancy hopping and rotation-assisted cation motion are still operative mechanisms (albeit at slower rates). The process is easily followed by variable-temperature ^{31}P NMR lineshape studies as reported here. The operative activation energy of 0.48 eV agrees well with the range of values (0.44−0.48 eV) extracted from the quadrupolar relaxation data at higher temperatures. This result suggests that the second-order phase transition occurring near 400 K does not fundamentally change the mechanism of cation transport but primarily accelerates the rate of process 1 in these materials.

Inspection of the parameters summarized in Tables 2 and 3 indicates that the timescales of both motional processes become increasingly similar with increasing vacancy concentration. For example, in the case of pure α-Na_3PO_4, the ratio of the correlation times of both processes is approximately 250:1, whereas for 25% Na_2SO_4 content, this ratio drops to 3.6:1. In the case of process 2 this is consistently explained in terms of a decreased average length of stay in a given site, resulting from the increased probability of a vacant site nearby. Furthermore, it is conceivable that this mechanism interferes with both the anion rotation and cation diffusion, which both get effectively slower. As a result the attempt frequency τ_{co}^{-1} is lowered with increasing x, as shown in Figure 15. However, to provide further evidence for this contention, and thereby prove the paddle-wheel mechanism, a detailed independent study of the anion dynamics is mandatory. To this end ^{17}O NMR experiments on isotropically enriched samples are currently in progress in our laboratory.[72]

Acknowledgment. Support of this work by the Ministerium für Wissenschaft und Forschung Nordrhein-Westfalen is gratefully acknowledged. We thank H., Freiheit for assistance with the X-ray diffractometric characterization of the solid solution samples, and Professors K. Funke, D. Wilmer, and A. Putnis (WWU Münster) and M. Jansen (MPI Stuttgart) for valuable discussions.

References and Notes

(1) Jansen, M. *Angew. Chem.* **1991**, *103*, 1574.
(2) Karlsson, L.; McGreevy, R. L. *Solid State Ionics* **1995**, *76*, 301.
(3) Lundén, A. *Solid State Ionics* **1988**, *28−30*, 163.
(4) Lundén, A. *Solid State Commun.* **1988**, *65*, 1237.
(5) Lundén, A.; Dissanayake, M. *J. Solid State Chem.* **1991**, *90*, 179.
(6) Lundén, A. *Solid State Ionics* **1994**, *68*, 77.
(7) Lundén, A. *Z. Naturforsch.* **1995**, *50a*, 1067.
(8) Secco, E. *Solid State Ionics* **1988**, *28−30*, 168.
(9) Secco, E. *Solid State Commun.* **1988**, *66*, 921.
(10) Secco, E. *Solid State Ionics* **1991**, *45*, 335.
(11) Secco, E. *J. Solid State Chem.* **1992**, *96*, 366.
(12) Secco, E. *Solid State Ionics* **1993**, *60*, 233.
(13) Funke, K.; Wilmer, D.; Banhatti, R. D.; Witschas, M.; Lechner, R. E.; Fitter, J.; Jansen, M.; Korus, G. *Mater. Res. Soc. Symp. Proc.* **1998**, *525*, 469.
(14) Wilmer, D.; Banhatti, R. D.; Fitter, J.; Funke, K.; Jansen, M.; Korus, G.; Lechner, R. E. *Physica B* **1998**, *241−243*, 338.
(15) Wilmer, D.; Funke, K.; Witschas, M.; Banhatti, R. D.; Jansen, M.; Korus, G.; Fitter, J.; Lechner, R. E. *Physica B* **1999**, *266*, 60.
(16) Brinkmann, D. *Prog. NMR Spectrosc.* **1992**, *24*, 527.
(17) Göbel, E.; Müller-Warmuth, W.; Olyschläger, H.; Dutz, H. *J. Magn. Reson.* **1979**, *36*, 371.
(18) Bjorkstam, J. L.; Villa, M. *Magn. Reson. Rev.* **1980**, *6*, 1.
(19) Grüne, M.; Müller-Warmuth, W.; zum Hebel, P.; Krebs, B. *Solid State Ionics* **1993**, *66*, 165.
(20) Junke, K. D.; Mali, M.; Roos, J.; Brinkmann, D.; Lunden, A.; Graneli, B. *Solid State Ionics* **1988**, *28−30*, 1287.
(21) Massiot, D.; Bessada, C.; Echegut, P.; Coutures, J. P.; Taulelle, F. *Solid State Ionics* **1990**, *37*, 223.
(22) Wiench, D. M.; Jansen, M. *Z. Anorg. Allg. Chem.* **1980**, *461*, 101.
(23) Wiench, D. M.; Jansen, M. *Z. Anorg. Allg. Chem.* **1982**, *486*, 57.
(24) Hruschka, H.; Lissel, E.; Jansen, M. *Solid State Ionics* **1988**, *28−30*, 159.
(25) Irvine, J. T. S.; West, A. R. *J. Solid State Chem.* **1987**, *69*, 126.
(26) van Vleck, J. H. *Phys. Rev.* **1948**, *54*, 682.
(27) Abragam, A. *Principles of Nuclear Magnetism*; Oxford Science Publishers: Oxford, 1961; p 111.
(28) Lissel, E.; Jansen, M.; Jansen, E.; Will, G. *Z. Kristallogr.* **1990**, *192*, 233.
(29) Gutowsky, H. S.; Pake, G. E.; Bersohn, R. *J. Chem. Phys.* **1954**, *22*, 643.
(30) Hendrickson, J. R.; Bray, P. J. *J. Magn. Reson.* **1973**, *9*, 341.
(31) Waugh, J. S.; Fedin, E. I. *Sov. Phys. Solid State* **1963**, *4*, 1633.
(32) Hubbard, P. S. *J. Chem. Phys.* **1970**, *53*, 985.
(33) Werbelow, L. G. *J. Chem. Phys.* **1979**, *70*, 5381.
(34) Werbelow, L. G.; Marshall, A. G. *J. Magn. Reson.* **1981**, *43*, 443.
(35) Marshall, A. G.; Bruce, R. E. *J. Magn. Reson.* **1980**, *39*, 47.
(36) Monoi, H. *Rev. Magn. Reson. Med.* **1986**, *1*, 73.
(37) Westlund, P.-O.; Wennerström, H. *J. Magn. Reson.* **1982**, *50*, 451.
(38) Tokuhiro, T. *J. Magn. Reson.* **1988**, *76*, 22.
(39) Einarsson, L.; Nordenskiöld, L.; Rupprecht, A.; Furó, I.; Wong, T. C. *J. Magn. Reson.* **1991**, *93*, 34.
(40) Bloembergen, N.; Purcell, E. M.; Pound, R. V. *Phys. Rev.* **1948**, *73*, 679.
(41) Geiger, A.; Hertz, H. G. *Adv. Mol. Relax. Processes* **1976**, *9*, 293.
(42) Medek, A.; Harwood, J. S.; Frydman, L. *J. Am. Chem. Soc.* **1995**, *117*, 12779.
(43) Fernandez, C.; Amoureux, J. P. *Solid State Nucl. Magn. Reson.* **1996**, *5*, 315.
(44) Ernst, R. R.; Bodenhausen, G.; Wokaun, A. *Principles of Nuclear Magnetic Resonance in One and Two Dimensions*; Oxford University Press: Oxford, U.K. 1987.
(45) Fernandez, C.; Amoureux, J. P.; Chezeau, J. M.; Delmotte, L.; Kessler, H. *Micropor. Mater.* **1996**, *6*, 331.
(46) Dollase, W. A.; Merwin, L. H.; Sebald, A. *J. Solid State Chem.* **1989**, *83*, 140.
(47) Eckert, H. *NMR−Basic Principles Prog.* **1994**, *33*, 131 (review) and references therein.
(48) Kentgens, A. P. M.; Lemmens, J. M. M.; Geurts, F. M. M.; Veeman, W. S. *J. Magn. Reson.* **1987**, *71*, 62.
(49) Becker, K. D. *Z. Naturforsch.* **1982**, *37a*, 697.
(50) Freude, E.; Haase, J. *NMR−Basic Principles Prog.* **1993**, *29*, 64.
(51) Becker, K. D.; Hamann, H.; Kozubek, N.; Richtering, H,. *Ber. Bunsen-Ges. Phys. Chem.* **1975**, *79*, 1124.
(52) Lerner, L.; Torchia, D. A. *J. Am. Chem. Soc.* **1986**, *108*, 4264.
(53) Davis, D., Ph.D. Dissertation, University of California, Santa Barbara, 1991.
(54) Butler, A.; Eckert, H. *J. Am. Chem. Soc.* **1989**, *111*, 2802.
(55) Aramini, J. M.; Saponja, J. A.; Vogel, H. J. *Coord. Chem. Rev.* **1996**, *149*, 193.
(56) Aramini, J. M.; Vogel, H. J. *J. Am. Chem. Soc.* **1994**, *116* (5), 1988.
(57) Aramini, J. M.; Germann, M. W.; Vogel, H. J. *J. Am. Chem. Soc.* **1993**, 115 (21), 9750.
(58) Kimura, K.; Satoh, N. *Chem. Lett.* **1989**, 271.
(59) Marshall, A. G.; Wang, T. Lin; Cotrell, C. E.; Werbelow, L. G. *J. Am. Chem. Soc.* **1982**, *104*, 7665.
(60) Springer, C. S. *Annu. Rev. Biophys. Chem.* **1987**, *16*, 375.
(61) Bull, T. E.; Forsen, S.; Turner, D. L. *J. Chem. Phys.* **1979**, *70*, 3106.
(62) Inagaki, Y.; Maekawa, H.; Yokokawa, T.; Shimokawa, S. *Phys. Rev. B* **1993**, *47*, 674.
(63) Bjorkstam, J. L.; Villa, M. *Phys. Rev.* **1980**, *B 22*, 5025.
(64) Villa, M.; Bjorkstam, J. L. *Phys. Rev.* **1980**, *B 22*, 5033.
(65) Bjorkstam, J. L.; Villa, M.; Farrington, G. C. *Solid State Ionics* **1981**, *5*, 189.
(66) Bjorkstam, J. L.; Terloni, P.; Villa, M. *J. Chem. Phys.* **1980**, *73*, 2932.
(67) Bailey, W.; Glowinkowski, S.; Story, H.; Roth, W. L. *J. Chem. Phys.* **1976**, *64*, 4126.
(68) Chung, I.; Story, H. S.; Roth, W. L. *J. Chem. Phys.* **1975**, *63*, 4903.
(69) Bottyan, L.; Dupree, R.; Chandrashekhar, G. V. *Solid State Ionics* **1983**, *9−10*, 347.
(70) George, A. M.; Stebbins, J. F. *Phys. Chem. Miner.* **1996**, *23*, 526.
(71) George, A. M.; Sen, S.; Stebbins, J. F. *Solid State Nucl. Magn. Reson.* **1997**, *10*, 9.
(72) Witschas, M.; Eckert, H.; Korus, G.; Jansen, M. To be published.